frontiers | Frontiers in Energy Research

TYPE Original Research
PUBLISHED 08 February 2023
DOI 10.3389/fenrg.2023.1094285

OPEN ACCESS

EDITED BY
Mark David DeHart,
Idaho National Laboratory (DOE),
United States

REVIEWED BY
Di Yun,
Xi'an Jiaotong University, China
Luteng Zhang,
Chongqing University, China

*CORRESPONDENCE
Kyle M. Paaren,
kyle.paaren@inl.gov

SPECIALTY SECTION
This article was submitted to Nuclear Energy, a section of the journal Frontiers in Energy Research

RECEIVED 09 November 2022
ACCEPTED 11 January 2023
PUBLISHED 08 February 2023

CITATION
Paaren KM, Gale M, Medvedev P and Porter D (2023), Evaluation of BISON metallic fuel performance modeling against experimental measurements within FIPD and IMIS databases. *Front. Energy Res.* 11:1094285. doi: 10.3389/fenrg.2023.1094285

Evaluation of BISON metallic fuel performance modeling against experimental measurements within FIPD and IMIS databases

Kyle M. Paaren*, Micah Gale, Pavel Medvedev and Douglas Porter

Idaho National Laboratory, Idaho Falls, ID, United States

Simulations were conducted using the BISON fuel performance code on an automated process to read initial and operating conditions from two databases—the Fuels Irradiation and Physics Database (FIPD) and Integral Fast Reactor Materials Information System (IMIS) database. These databases contain metallic fuel data from the Experimental Breeder Reactor-II (EBR-II) and the Fast Flux Test Facility (FFTF). The work demonstrates use of an integrated framework to access EBR-II fuel pin data for evaluating fuel performance models contained within BISON to predict fuel performance of next-generation metallic fuel systems. Between IMIS and FIPD, there is enough information to conduct 1,977 unique EBR-II metallic fuel pin histories from 29 different experiments, and 338 pins from FFTF MFF-3 and MFF-5 with varying levels of details between the two databases. Each of these fuel performance histories includes a high-resolution power history, flux history, coolant channel flow rates, and coolant channel temperatures, and new model developments in BISON since the initial demonstration of this integrated framework. Fission gas release (FGR), cumulative damage fraction, fuel axial swelling, FCCI wastage thickness, cladding profilometry, and burnup were all simulated in BISON and compared to post-irradiation examination (PIE) results to evaluate BISON fuel performance modeling. Implementation of new fuel performance models into a generic BISON input file coupled with IMIS and FIPD yielded results with a better representation of physics than the initial evaluation of the integrated framework. Cladding profilometry, FGR, and fuel axial swelling were found to be in good agreement with PIE measurements for most of the pins simulated. The chosen mechanical contact solver was found to significantly impact the axial fuel swelling and cladding strain predictions when used in conjunction with the U-Pu-Zr hot-pressing model since it bound the fuel to prevent further swelling and increased hydrostatic stresses. This work suggests that fuel performance modeling in BISON under steady-state conditions represents the PIE data well and should be reassessed when new PIE data become available in IMIS and FIPD databases and when improved physical models to better capture fuel performance are added to BISON.

Abbreviations: ANL—argonne national laboratory; EBR-II—experimental breeder reactor-II; FCCI—fuel cladding chemical interaction; FCMI—fuel cladding mechanical interaction; FFTF—fast flux test facility; FGC—fission gas collected; FGP—fission gas produced; FGR—fission gas release; FIPD—fuels irradiation and physics database; GLASS—germanium-lithium argon-scanning system; HFEF—hot fuel examination facility; IMIS—integral fast reactor materials information system; INL—idaho national laboratory; LHGR—linear heat generation rate; MFF—mechanistic fuel failure; MOOSE—multiphysics object-orientated simulation environment; PIE—post-irradiation examination; SEE—Standard error of the estimate; SMR—small modular reactor; VTR—versatile test reactor.

KEYWORDS
BISON, metallic fuel, simulation, validation, assessment

Introduction

With the recent advances in development of Small Modular Reactors (SMRs) and the framework for their licensing, there is growing need to have a greater understanding of metallic fuels and associated fuel pin failure rates (Crawford et al., 2018; Williamson et al., 2021). The Versatile Test Reactor (VTR) will perform the necessary experiment scale tests to aid in acquisition of experimental data to provide insight for the development of next-generation nuclear reactors such as those being conceptualized by TerraPower and Oklo (Crawford et al., 2018). To prepare BISON to help the VTR and other next-generation reactor testing programs, BISON has been paired with the Fuels Irradiation and Physics Database (FIPD) and Integral Fast Reactor Materials Information System (IMIS), which supply post-irradiation examination (PIE) and fuel pin data from Experimental Breeder Reactor (EBR) II and Fast Flux Test Facility (FFTF) MFF-3 and 5 (Yacout et al., 2017; Oaks et al., 2019; Porter and Mariani, 2019). With the databases linked to BISON, proper assessment cases can be used to validate metallic fuel models within the BISON code (Paaren et al., 2021a). This work attempts to replicate the behavior and benchmark 29 EBR-II experiments with PIE data supplied through IMIS and FIPD, with an evaluation of BISON predicted burnup, axial fuel swelling, fission gas release (FGR), and cladding profilometry. Since the initial demonstration of the integrated framework, significant advances within BISON's metallic fuel performance modeling have been made, such as the inclusion of void swelling of cladding materials, integration of fuel cladding chemical interaction (FCCI) effects, capturing frictional contact, and integrating hot-pressing of U-Pu-Zr fuel to correct the overprediction of fuel swelling (Paaren et al., 2021b; Paaren et al., 2021c). These mechanics, with the exception of hot-pressing, were implemented in all 1,977 EBR-II BISON simulations so fuel performance for next-generation reactors can be evaluated.

Until relatively recently, Idaho National Laboratory (INL) and Argonne National Laboratory (ANL) have developed IMIS and FIPD to store EBR-II and FFTF MFF data for easy access in order to support model development and validation activities (Yacout and Billone, 2017; Yacout et al., 2017; Oaks et al., 2019; Porter and Mariani, 2019). Note that much of these data have yet to be qualified for use for fuel qualification. ANL is in the process of qualifying data to Nuclear Quality Assurance standards (Yacout and Billone, 2017). Each of these databases includes crucial reactor conditions needed to properly simulate a fuel pin within BISON. These reactor conditions include axial power and flux profiles for individual pins, average and the max linear heat generation rate (LHGR) for each operating cycle, reactor power, flux and fluence histories, and coolant boundary conditions. These reactor conditions from FIPD are read directly into the BISON fuel performance simulations for each fuel pin. Access to the reactor conditions used for each fuel pin in this work is controlled by Argonne National Laboratory (Yacout and Billone, 2017; Yacout et al., 2017; Oaks et al., 2019; Porter and Mariani, 2019). In addition to these reactor conditions, geometric dimensions and compositions of each pin are available, which will be used in this work for the inputs for the BISON fuel performance simulations (Yacout et al., 2017; Oaks et al., 2019; Porter and Mariani, 2019). PIE measurements available for BISON model comparison in this work includes 551 digitized cladding profilometry scans, 1,333 axial fuel swelling measurements, and 168 FGR measurements for EBR-II pins. Also available with this PIE collection from IMIS and FIPD are gamma scans, neutron radiograph, gas chemistry, irradiated pin weights, and laser profilometry measurements.

BISON, a finite element method code, is based off the Multiphysics Object-Orientated Simulation Environment (MOOSE). This allows users to create C++ objects for tightly coupled simulations, such as void swelling models (Williamson et al., 2016). BISON is capable of predicting fuel performance for a variety of fuel forms including light-water reactor fuel rods and metallic fuel (Medvedev, 2012; Hales et al., 2014). BISON solves the fully coupled thermomechanical equations and species diffusion for varying geometry. Fuel models within BISON include temperature, porosity, and burnup-dependent thermal properties, along with models that describe fuel behavior such as swelling from FGR (Galloway and Matthews, 2016). Mechanical and thermal contact were also modeled to allow for thermomechanical coupling and cladding profilometry comparisons with PIE data. The primary benefit of using BISON compared to other fuel performance codes is that BISON users can contribute their own C++ objects to the code and develop models BISON, such as void swelling correlations, FCCI correlations, and zirconium redistribution presented in prior works (Galloway, 2015; Matthews et al., 2017; Paaren et al., 2021b; Paaren et al., 2021c).

The irradiation-induced volumetric swelling models added into the BISON code were based off EBR-II and FFTF MFF fuel pins from the irradiation experiments. There have been multiple iterations and updates to these equations over the years, which were originally developed to predict the cladding strain and volumetric swelling of cladding while in a reactor system (Garner and Porter, 1988; Briggs et al., 1995; Garner, 2017; Hofman et al., 2019). Each of the volumetric swelling correlations depend on the volume change due to void formations and thermal precipitation-based densification, with SS316 having no thermal densification term (Garner and Porter, 1988; Briggs et al., 1995). Each correlation is dependent on temperature and fluence in the cladding material to predict the volumetric swelling. Time-dependent forms of these equations were utilized to allow users to integrate over the operating cycles of a reactor to capture time-dependent changes in-reactor operating conditions. These equations are shown in Eqs 1–11. Implementation of volumetric void swelling models for cladding materials was found to give BISON an improvement in cladding profilometry predictions for HT9, D9, and SS316 cladding for EBR-II experiments X421, X441, and X486 (Paaren et al., 2021b). These same equations were used in this work to evaluate all EBR-II pins available within the aforementioned databases. $\dot{S}_0$ is the fractional volume rate of change due to void swelling, and $\dot{D}$ is the fractional volume rate of change due to solid swelling. R is the swelling rate parameter, and varies for each cladding type, which is also true for the incubation parameter τ, and the curvature parameter α (Briggs

TABLE 1 Swelling constants and units.

Parameter	Constant and units	HT9	D9	SS316
Incubation Parameter	τ $10^{22}\frac{n}{cm^2 s}$	14.2	11.9	$6.58 - 0.566\beta$ $T < 848\ K$
				$4.3105 + 2.46\beta$ $T \geq 848\ K$
Curvature Parameter	α $10^{22}\frac{cm^2}{n}$	0.75	0.75	0.75

et al., 1995; Hofman et al., 2019; Paaren et al., 2021b). Temperature is in Kelvin, and neutron flux is in units of 10^{22}. Constant values and units for each cladding are available in Table 1.

$$\text{HT9}\ \frac{d\frac{\Delta V}{V_0}}{dt} = \dot{V} = \dot{S}_0 + \dot{D} \tag{1}$$

$$\text{D9}\ \frac{d\frac{\Delta V}{V_0}}{dt} = \dot{V} = \dot{S}_0 - \dot{D} \tag{2}$$

$$\text{SS316}\ \frac{d\frac{\Delta V}{V_0}}{dt} = \dot{V} = \frac{S_0}{(1 - S_0)^2} \tag{3}$$

$$\text{SS316}\ R = e^{\left(0.497 + 0.795\beta - 0.0948\beta^2 + 0.908\beta^3 - 1.49\beta^4\right)} + e^{\left(-8\left(\beta - 1.35\right)^2\right.} \tag{4}$$

$$\text{HT9}\ R = 0.085e^{\left(-0.0001\left(T - 673.15\right)^2\right)} \tag{5}$$

$$\text{D9}\ R = 2.76e^{\left(-0.00017\left(T - 773.15\right)^2\right)} \tag{6}$$

$$\text{SS316}\ \beta = \frac{T - 773}{100} \tag{7}$$

$$\text{All}\int \dot{V}dt = \sum \dot{V}dt = \frac{\Delta V}{V_0} \tag{8}$$

$$\text{All}\ \frac{dS_0}{dt} = \dot{S}_0 = \frac{0.01\phi Rt}{1 + e^{\alpha\left(\tau - \phi t\right)}} \tag{9}$$

$$\text{HT9}\ \frac{dD}{dt} = \dot{D} = 1.5 \cdot 10^{-4}\phi e^{-0.1\phi t} \tag{10}$$

$$\text{D9}\ \frac{dD}{dt} = \dot{D} = 0.3\phi e^{-30\phi t}\left(-1.7 \cdot 10^{-4}T + 0.241\right). \tag{11}$$

A model for FCCI from the LIFE-METAL fuel performance code has been previously implemented into BISON to estimate the wastage thickness formed on the interface between the metallic fuel and the cladding interior surface. It allows for the wastage to be calculated using time-at-temperature and either flux, burnup, or a combination of the two for HT9, D9, and SS316 cladding. These empirical correlations are seen in Eqs 12–14, with the coefficients fitted based on PIE data from EBR-II experiments. Within Eqs 12–14, ϕ is neutron flux, B is the at% burnup, R is the gas constant, T is temperature in Kelvin, and D_0, Q, k_0, and D_{i0} are empirical constants. Note that the burnup and flux-burnup empirical models are aonly available for HT9 cladding. Within this work, only the flux dependent model was used. These models and coefficients used may all be found within the BISON documentation and the work which they were derived in and in Table 2 (Hales et al., 2015; Paaren et al., 2021b). These same coefficients were also used in prior works (Galloway, 2015; Matthews et al., 2017; Paaren et al., 2021b; Paaren et al., 2021c). The flux mode was calibrated using a variety of EBR-II experiments where the burnup and flux-burnup modes were calibrated using only experiment X447 due to the high temperatures exhibited within the experiment (Carmack, 2012; Hales et al., 2015). To represent FCCI, these equations were used in conjunction with continuum damage mechanics to mimic the thinning of the cladding wall by applying an enhanced effective stress (Paaren et al., 2021c). The damage from FCCI results in a reduction in the effective stiffness of the material,

TABLE 2 Wastage constants and units.

Constant and units	HT9	D9	SS316
k_0 $\frac{m}{s^{0.5}}$	39.13	N/A	N/A
Q_b $\frac{J}{mol}$	252253	N/A	N/A
Q $\frac{J}{mol}$	201782	266102	266102
D_0 $\frac{m^2}{s}$	$1.122 \cdot 10^{-4}$	7.885	2.419
D_{10} m^4	$1.792 \cdot 10^{-39}$	$6.398 \cdot 10^{-38}$	$1.953 \cdot 10^{-38}$

and, in its simplest form, the fractional reduction in stiffness can be represented by a scalar damage index between 0 (undamaged state) and 1 (fully damaged) for a material. The implementation of continuum damage mechanics for FCCI in high temperature experiments such as EBR-II X447 allowed for significant improvement in cladding profilometry predictions for D9 and HT9 clad pins (Paaren et al., 2021c).

$$\text{FCCI Flux Dependent}\ \frac{\Delta w}{\Delta t} = \frac{1}{2}\left(D_0 e^{-\frac{Q}{RT}} + D_{i0}\phi\right)^{\frac{1}{2}} t^{\frac{-1}{2}} \tag{12}$$

$$\text{FCCI Burnup Dependent}\ \frac{\Delta w}{\Delta t} = 2B\left(k_0 e^{-\frac{Q_b}{RT}}\right) t^{\frac{-1}{2}} \tag{13}$$

$$\text{FCCI Flux} - \text{Burnup Dependent}\ \frac{\Delta w}{\Delta t} = 2B\left(D_0 e^{-\frac{Q}{RT}} + D_{i0}\phi\right)^{\frac{1}{2}} t^{\frac{-1}{2}}. \tag{14}$$

Within this work, it will be described how the data for 1,977 EBR-II experimental pins are compared to empirical fuel performance correlations from the databases to evaluate current metallic fuel performance models with advances in metallic fuel models from prior works. With the IMIS and FIPD databases, BISON models were created that encompassed a power and flux history, variable flowrates throughout each operating cycle, and as-fabricated dimensions. These models were compared to digitized PIE data for burnup, FGR, fuel axial swelling, and cladding profilometry. The 1,977 fuel pin models developed were compared with all PIE data available and were provided along with statistical assessment and discussion. To do this, the two databases were fed into a Python 3.8 script to create the BISON input files in order to compare the BISON simulation results to PIE data.

Methods

The integrated framework between BISON and the two databases demonstrated in prior work is utilized in combinations with advances in BISON metallic fuel performance models to simulate and evaluate 1,977 EBR-II fuel pins (Paaren et al., 2021a). Improvements to the

integrated framework include utilizing FIPD generated power, flux, and coolant flowrate histories similar to how reactor operating histories were parsed in the initial integrated framework (Paaren et al., 2021a). New material model advancements within the BISON code have been added to the integrated framework as well. The general BISON input file for an EBR-II pin fuel performance simulation is discussed, along with relevant EBR-II data available to be compared with simulation predictions. Methods for PIE comparison with simulation data are discussed.

General solution

All BISON simulations used in this work are based on an evolving EBR-II input file with the latest BISON fuel performance models, with FIPD data and reactor conditions written into the simulations for each individual pin. In total, the following process produced 1,977 BISON simulations for the current fuel pin data found within FIPD. Generic scripts were developed within Python to update and create new EBR-II simulations to compare fuel performance predictions to experimental measurements. Each BISON model consisted of 2D-RZ geometry to take advantage of axial symmetry. An aspect ratio of 25.18 was used to mesh the fuel and cladding in each BISON simulation due to fast convergence of each simulation with no artifacts in the results. The SmearedPelletMesh meshing scheme creates a mesh encompassing a fuel slug and cladding, with dimensions, axial elements, and horizontal elements being specified. This meshing scheme was used as it allows BISON to create the mesh directly. All reactor condition functions within the BISON simulations were supplied by FIPD using linear interpolation between timesteps to approximate power, flux, and flowrates. At the very end of each fuel pin irradiation, the modeled coolant temperature is set to 20°C for room temperature conditions, and the LHGR and neutron flux are set to zero to end power production and irradiation to mimic PIE measurement conditions. This is important as all PIE data were collected and measured under these conditions within the Hot Fuel Examination Facility (HFEF) facility at INL the volumetric heat source used in the EBR-II fuel pin simulations relies on coupling the fission reaction rate and LHGR history to calculate power generated in the fuel slug. The fission reaction rate is computed by applying the axial profile, dimensions, and LHGR profile of each fuel pin. These values were calculated from the Physics Analysis Database which is then fed into FIPD.

Mechanical and thermal contact were implemented in the BISON EBR-II fuel pin simulations to allow for gap conductance heat transfer and Fuel Cladding Mechanical Interaction (FCMI). Thermal contact was allowed from the outer surface of the fuel to the inside wall of the cladding to transfer heat, with a temperature-dependent thermal conductivity sodium gap between the outer fuel surfaces and inside the cladding (Fink and Leibowitz, 1995). As the fuel expands, swells, and contacts the cladding, sodium is forced out of the gap and heat is directly transferred to the cladding wall. GapHeatTransfer was used to account for this and to transfer heat between the fuel and the cladding wall. The gap conductance method displaces sodium into the plenum region to account for the expansion of the metallic fuel. Mechanical contact used Augmented Lagrange frictional contact for all simulations with a friction coefficient of $\mu = 0.2$ based off previous work (Paaren et al., 2021c). The contact solver chosen within BISON affects the forces exhibited on the fuel and cladding after FCMI occurs and the fuel continues to swell, which helps prevent excess axial fuel swelling by binding the fuel. The anisotropic factor used within the gaseous fuel swelling model, ranging from 0.24 to 0.9, is dependent on plutonium content (Karahan, 2010; Paaren et al., 2021c). Currently, this has little physical basis, but allows for a variable parameter to better fit the difference between radial and axial swelling.

Several boundary conditions were used for the BISON EBR-II fuel pins, which include fixing all surfaces on the axial line of symmetry with a Dirichlet condition. This sets the radial displacements to zero at those surfaces so no elongation or swelling occurred over the axial boundary line. The bottom of the cladding and fuel were given a Dirichlet condition, setting all axial displacements to zero at those surfaces. Doing so allows for a reference point to be established for swelling deformation. The pressure of the sodium coolant channel was set to a constant 0.151 MPa on the outside of the cladding (Galloway and Matthews, 2016). Initially, the internal plenum pressure of 0.086 MPa was applied to the fuel's outer surfaces and the inner surfaces of the cladding, and released fission gas was added as a function of fuel burnup to the plenum volume to create a new pressure (Galloway and Matthews, 2016). Material models used to describe material properties for the fuel and the cladding are listed in Table 3 with the corresponding BISON object. Documentation over blocks used within the BISON EBR-II fuel pin simulations may be found in the BISON documentation and BISON user's manual (Hales et al., 2015).

EBR-II pin information and post-irradiation examination data

The 1,977 pin simulations are spread across 29 experiments in EBR-II, with some fuel pins being involved in multiple irradiation cycles of experiments. Each of the EBR-II experiments performed was used to investigate various phenomena that occur within U-Pu-Zr fuel, such as FCCI in X447, FCMI with different smeared densities in X441, and EBR-II driver fuel qualifications in X448 and X486. Most of the experiments within EBR-II contained sub-experiments, such as X425 having subsequent irradiations labeled X425A, X425B, and X425C. During the operating cycles between each experiment, pins were pulled for axial growth and profilometry measurements, axial gamma scanning, and neutron radiography. These pins were then reloaded into new assembly hardware to be re-irradiated. This process allowed insight on time or burnup dependent fuel performance phenomena as irradiation progresses. In addition, multiple datapoints for a singular fuel pin allows for a larger dataset used in this evaluation of fuel performance models. A list of all available 29 EBR-II experiments detailing fuel and cladding types used is provided in Table 4.

Irradiation conditions, including pin-specific power and flux, axial power and flux profiles, coolant conditions, and as-designed and as-fabricated dimensions of each fuel slug and cladding within EBR-II is obtained from FIPD (Yacout and Billone, 2017; Yacout et al., 2017; Oaks et al., 2019; Porter and Mariani, 2019). These irradiation conditions are written into each BISON simulation and follow the reactor power history contained within the GLASS data. The fidelity of the GLASS data allows for the power and flux histories of EBR-II pins to change every 60 s and is used within these simulations. The irradiation conditions used within the

TABLE 3 BISON Objects used in BISON Simulations (Hales et al., 2015).

Phenomenon	Fuel	Cladding
Fuel Phase	PhaseUPuZr (Galloway et al., 2015)	N/A
Thermal Conductivity	ThermalUPuZr (Billone et al., 1968) (Savage, 1968)	ThermalHT9 (Hofman et al., 2019) (Yamanouchi et al., 1992)
		ThermalD9 (Hofman et al., 2019) (Banerjee et al., 2007) (Leibowitz and Blomquist, 1988)
		Thermal316 (Mills, 2002)
Density ($g{\cdot}cm^{-3}$)	15.8	7.8
Burnup	UPuZrBurnup (Olander, 1976)	N/A
Fission Rate	UPuZrFissionRate (Hales et al., 2015)	N/A
Elasticity Tensor	UPuZrElasticityTensor (Hofman et al., 2019)	HT9ElasticityTensor (Los Alamos National Laboratory, 2014)
		D9ElasticityTensor (Hofman et al., 2019)
		SS316ElasticityTensor
Creep	UPuZrCreepUpdate (Hofman et al., 2019)	HT9CreepUpdate (Hofman et al., 2019)
		D9CreepUpdate (Hofman et al., 2019)
		SS316CreepUpdate (Altenbach and Gorash, 2013) (Garner and Porter, 1988)
Thermal Expansion	UPuZrThermalExpansionEigenstrain (GeelHood and Porter, 2018)	HT9ThermalExpansionEigenstrain (Leibowitz and Blomquist, 1988)
		D9ThermalExpansionEigenstrain (Hofman et al., 2019) (Leibowitz and Blomquist, 1988)
		SS316ThermalExpansionEigenstrain (American Society of Mechanical Engineers, 2016) (Niffenegger and Reichlin, 2012)
Gaseous Swelling	UPuZrGaseousEigenstrain (Olander, 1976) (Karahan, 2010)	N/A
Fission Gas Release	UPuZrFissionGasRelease (Hofman et al., 1997)	N/A
Solid Swelling	BurnupDependentEigenstrain (Ogata and Takeshi, 1999)	N/A
Cladding Void Swelling	N/A	SS316VolumetricSwellingEigenstrain (Briggs et al., 1995)
		HT9VolumetricSwellingEigenstrain (Hofman et al., 2019)
		D9VolumetricSwellingEigenstrain (Hofman et al., 2019)
FCCI	N/A	MetallicFuelWastage (Hales et al., 2015)
		MetallicFuelWastageDamage (Hales et al., 2015)
CDF	N/A	FailureCladHT9 (Karahan and Buongiorno, 2010)
		FailureCladD9 (Briggs et al., 1995)

BISON simulations are available upon request and with access granted by ANL. Note that FIPD data is currently being merged into the BISON code, with plans to have dual BISON and FIPD users to have access to these irradiation conditions directly and simulate any of these assessment cases.

EBR-II PIE data within IMIS and FIPD used in this study included 1,337 axial swelling measurements, 551 cladding profilometry contact roller measurements, and 168 FGR measurements. In addition to this, FIPD provides calculated peak and average burnups, fuel temperatures, and cladding temperatures for each fuel pin during each operating cycle. These calculated parameters serve as a comparison for BISON predictions. The PIE data were usually measured within the HFEF facility at INL, with an internal temperature around 300 K. This is important, as the EBR-II fuel pins simulated in BISON need to be brought to 300 K for a direct comparison with PIE measurements. To do so, the LHGR history in BISON was set to zero after irradiation was completed, and the coolant channel temperature was set to 300 K. Uncertainty analyses for the BISON simulations and PIE data were not possible because uncertainties in the data and reactor conditions were not available. It is recognized that some models used in the conducted BISON simulations use empirical equations to describe phenomena, and occasionally expert bias may be present when performing measurements for PIE data, particularly axial fuel growth. This particularly refers to historical axial swelling measured by hand from neutron radiographs; however, new efforts have yielded implementation of image recognition software to determine axial swelling measurements from digitized radiographs (V Gribok et al., 2021).

TABLE 4 Pin information.

Experiment	Fuel Type(s)	Number of unique pins[a]	Cladding Type(s)	Peak linear power ($kW \cdot m^{-1}$)	Peak cladding temperature (K)	Peak fuel temperature (K)	Burnup (at%)	Fast fluence (10^{22} $n \cdot cm^2$)
X419	U-10Zr	89	D9	51.18	833.15	1007.15	12.41	12.01
	U-19Pu-10Zr							
	U-8Pu-10Zr							
X420	U-10Zr	80	D9	47.90	859.15	1003.65	18.13	18.54
	U-19Pu-10Zr							
	U-8Pu-10Zr							
X421	U-10Zr	80	D9	47.90	820.15	978.15	18.96	19.7
	U-19Pu-10Zr							
	U-8Pu-10Zr							
X423	U-10Zr	82	316SS	43.96	773.15	963.15	5.22	8.08
	U-19Pu-10Zr							
	U-22Pu-10Zr							
	U-26Pu-10Zr							
	U-3Pu-10Zr							
	U-8Pu-10Zr							
X425	U-10Zr	92	HT9	48.23	880.58	1000.58	19.9	20.67
	U-19Pu-10Zr							
	U-8Pu-10Zr							
X429	U-10Zr	65	316SS	45.93	843.58	986.15	14.18	13.86
	U-19Pu-10Zr		HT9					
	U-8Pu-10Zr							
X430	U-10Zr	52	HT9	50.85	864.58	1010.15	11.83	18.11
	U-19Pu-10Zr							
	U-22Pu-10Zr							
	U-26Pu-10Zr							
X431	U-10Zr	22	HT9	39.37	859.58	915.15	4.36	15.02
	U-2Zr							
	U-6Zr							
X432	U-10Zr	21	HT9	40.35	867.15	925.15	4.69	16.25
	U-2Zr							
	U-6Zr							
X435	U-10Zr	115	D9	47.90	803.15	918.15	20.21	22.28
X441	U-10Zr	72	D9	54.13	852.15	1039.15	12.91	10.11
	U-19Pu-10Zr							
	U-19Pu-14Zr							
	U-19Pu-6Zr							

(Continued on following page)

TABLE 4 (*Continued*) Pin information.

Experiment	Fuel Type(s)	Number of unique pins[a]	Cladding Type(s)	Peak linear power ($kW \cdot m^{-1}$)	Peak cladding temperature (K)	Peak fuel temperature (K)	Burnup (at%)	Fast fluence (10^{22} $n \cdot cm^2$)
X447	U-10Zr	53	D9	36.42	930.58	1000.15	9.99	9.18
			HT9					
X448	U-10Zr	68	HT9	46.59	807.15	918.15	14.79	14.89
X449	U-10Zr	61	HT9	32.81	846.58	911.58	11.44	10.55
X450	U-10Zr	61	HT9	36.09	869.15	940.15	10.25	9.51
X451	U-10Zr	65	HT9	35.43	916.58	983.15	12.92	12.06
X452	U-10Zr	61	D9	34.12	852.15	923.15	6.07	5.39
X453	U-10Zr	61	D9	34.12	845.58	917.15	9.35	8.46
X454	U-10Zr	61	D9	49.54	808.15	927.15	9.14	9.13
X455	U-10Zr	61	D9	50.20	810.15	933.15	9.18	9.17
X482	U-10Zr	123	316SS	40.68	890.58	967.15	14.92	14.73
	U-19Pu-10Zr		D9					
			HT9					
X483	U-10Zr	107	316SS	48.23	818.15	930.15	15.09	15.7
X484	U-10Zr	61	316SS	33.79	842.15	912.15	11.65	10.68
X485	U-10Zr	61	316SS	38.39	865.58	942.15	10.74	10.22
X486	U-10Zr	109	316SS	39.04	918.58	992.15	12.6	12.27
X489	U-10Zr	61	HT9	35.10	864.58	991.15	5.47	4.83
	U-19Pu-10Zr							
	U-28Pu-10Zr							
X492	U-10Zr	71	316SS	41.34	840.58	960.15	9.03	8.82
	U-19Pu-10Zr							
	ZR-U-10Zr							
	ZR-U-19Pu-10Zr							
X496	U-10Zr	37	HT9	61.68	794.15	982.15	5.95	4.15
X501	U-10Zr	61	316SS	46.46	790.58	955.15	4.72	4.24
	U-20.3Pu-1.3Np-2.1Am-10Zr		HT9					

[a]Includes replacement pins for those destructively examined during an interim experiment exam.

Simulation and post-irradiation examination comparison

For comparing BISON simulations to PIE data, BISON postprocessors and vector postprocessors were written to csv files to be read into Python. PIE profilometry data obtained from FIPD was read into Python from csv files as well. It is important to note that much of the EBR-II cladding contact profilometry PIE data was digitized by ANL from data directedly recorded to chart paper and is being qualified to Nuclear Quality Assurance quality standards. PIE measurements compared to BISON simulations include FGR, cladding profilometry, and fuel axial swelling, along with calculated burnup. These measurements and calculations were compared within Python, with statistical analysis performed. Standard deviations were provided for single value measurements, such as FGR, burnups, and axial fuel swelling. For cladding profilometry, the standard error of the estimate (SEE) was used as it takes into account the axial shift of the profiles by accounting for the differences between the two sets of data, as seen in Figure 1 and Eq. 11, with y being the BISON clad displacement, $\hat{y}$ being the PIE clad displacement, and n being the number of profilometry datapoints for each pin (Cohen, 1988; Everitt and Skrondal, 2010). For each axial height within the cladding

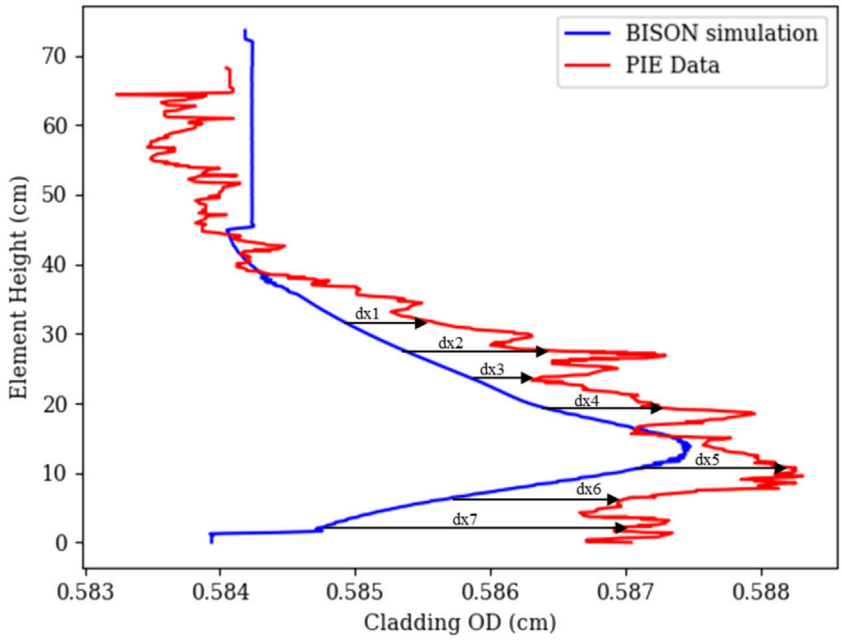

FIGURE 1
Profilometry profile statistical assessment with Standard Error of the Estimate (Paaren et al., 2021b; Paaren et al., 2021c).

profilometry PIE, the difference between the measured cladding diameter and BISON prediction was taken, then squared and summed, then divided by the number of axial positions for each pin to obtain the particular pin variance. For each pin's SEE value, the square root of the variance was taken.

$$SEE = \sqrt{\frac{\sum (y - \hat{y})^2}{n - 2}}. \tag{11a}$$

The cladding profilometry SEE, axial fuel swelling, calculated burnup, and FGR errors between the BISON simulations and PIE data were calculated for each pin among the 1,977 pins simulated in BISON. In addition to pin-wise statistics, the cladding profilometry SEE values for all 551 pins were reported to evaluate the cladding strain for various fuel and cladding types. A single value for SEE encompassing all 551 pins was reported along with the standard deviation. Creep is included in the cladding profilometry for both modeling and PIE data, the variability of which could affect the differences between the two in addition to differences caused from FCMI and FCCI. The oscillations seen within the experimental measurements is due to how contact profilometry is performed. Traditionally, mechanical rollers are used and roll along the outer diameter of the cladding. Small spikes and oscillations may occur due to dirt and debris being on the cladding wall during PIE measurements, or from manufacturing tolerances of EBR-II cladding, which was ±0.0005" (0.00127 cm) (Paaren et al., 2021b; Paaren et al., 2021c).

Results

To illustrate the capabilities developed, 1,977 pins were simulated within BISON from 29 different EBR-II experiments that applied operating conditions obtained from IMIS and FIPD for each pin. The pins discussed in the results below represent different smeared densities, irradiation lengths of time, cladding materials, fuel compositions, and linear heat rates to demonstrate how BISON and the databases can assess different metallic fuel pins that undergo different conditions. Burnup results obtained from BISON simulations were in agreement with IMIS and FIPD values. Cladding profilometry simulation results presented in this section were compared to PIE cladding profilometry, with SEE provided for each of the 551 pins. The highest SEE values observed were 85% smeared density pins, due to BISON overpredicting FCMI. FGR from BISON simulations were predicted around 70%, where 81 PIE FGR measurements did not exceed 73% on average. Implementation of frictional contact allowed for better BISON predictions for axial fuel elongation, with most for the 1,337 pins underpredicting PIE measurements by 1.2 cm. Overall, the development of new BISON material models and fitting of empirical coefficients has significantly improved the predictability of BISON to model metallic fuel performance.

Burnup

The average burnup values obtained from all BISON simulations were compared to FIPD, with the difference between the two values displayed in Figure 2. The difference in peak burnup values between the BISON simulations and FIPD are displayed in Figure 3. Because the reactor power history data were written into the BISON input files, excluding the short durations of power reduction and ascension at the beginning and end of the operating cycles (as explained earlier in this paper), burnup rate is fairly constant over time, with deviation form linearity at burnups exceeding 10 at%. This also contributes to BISON underpredicting

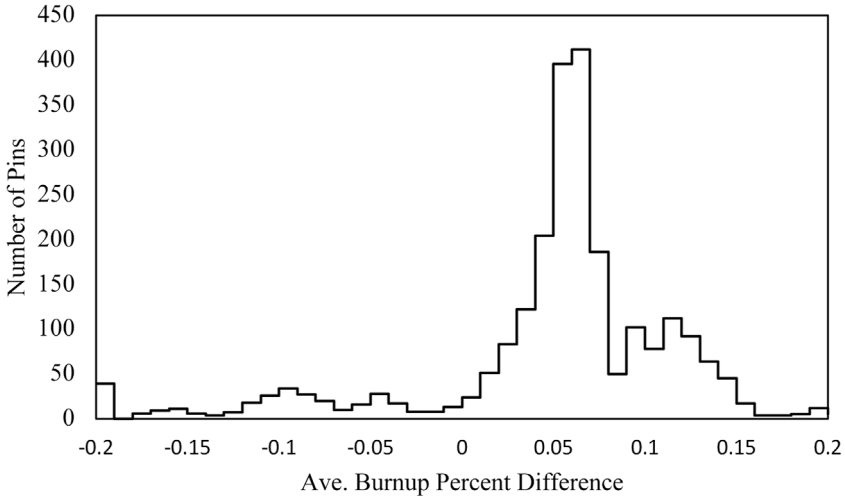

FIGURE 2
Difference in average burnup between BISON and Fuels Irradiation and Physics Database (BISON subtracted from FIPD).

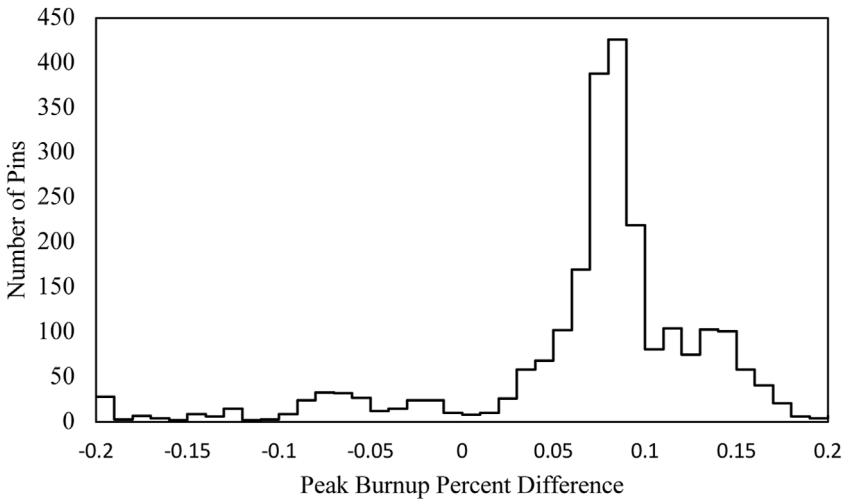

FIGURE 3
Difference in peak burnup between BISON and Fuels Irradiation and Physics Database (BISON subtracted from FIPD).

the burnup of most pins by 5%. The energy per fission assumed within the BISON simulations was 3.2×10^{-11} J. This assumption breaks down for non-plutonium bearing pins and higher enriched uranium fuel, both of which EBR-II are contained within EBR-II. This is due to the energy released per fission being unique to each isotope in the fuel. Accounting for plutonium production, isotopic enrichment, and decay in the BISON simulations would lead to better agreement between FIPD and the BISON simulations, as the increased energy per fission would lead to a higher burnup by ~5% due to the increased energy per fission (210 Mev for ^{239}Pu and 200 Mev for ^{235}U). Likewise, BISON peak burnup would increase from this as well, but at different rate due to plutonium bearing and non-plutonium bearing fuel. This is seen in Figure 4, with two distinct peaks formed.

Differences in peak burnup values between BISON and FIPD were larger than average burnup values due to not accounting for zirconium redistribution within the modeling efforts. Allowing zirconium to redistribute within the fuel matrix creates a zirconium depletion zone in the beta-phase of fuel, which is then filled with uranium migrating from the gamma and alpha phases. This creates a uranium rich zone leading to increased local fission rates and burnup. Overall, BISON is able to accurately predict average burnup results of metallic fuel with the current burnup material model in the BISON code after accounting for plutonium breeding and initial isotopic enrichment. Adding zirconium redistribution into BISON simulations would increase peak burnup, allowing for better agreement with FIPD burnup values. In each case, BISON simulations underpredicted peak burnup. This was expected due to zirconium redistribution

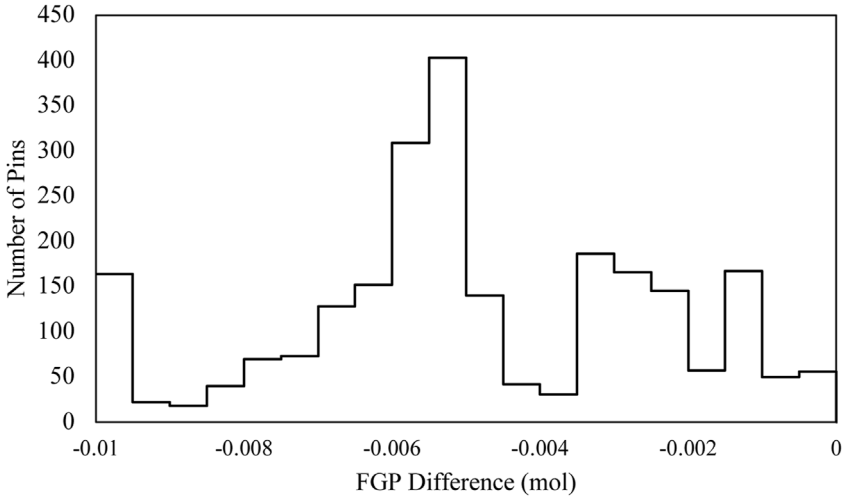

FIGURE 4
Fission gas produced comparison (BISON subtracted from FIPD).

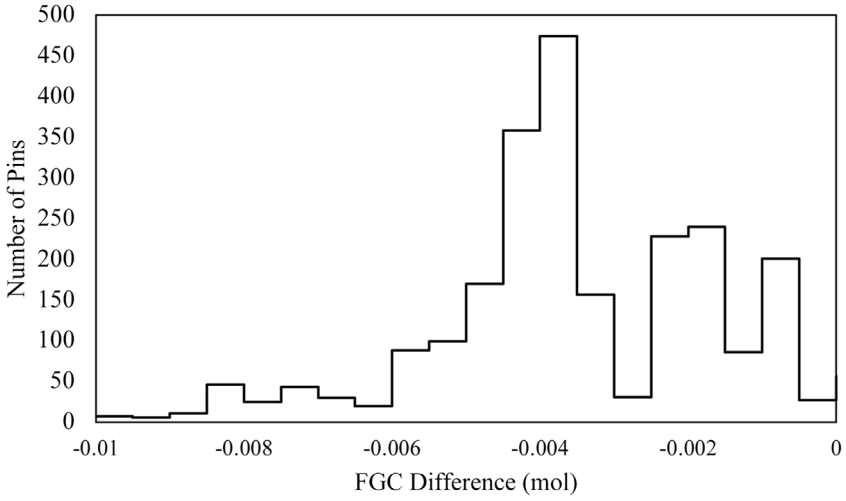

FIGURE 5
Fission gas collected comparison (BISON subtracted from FIPD).

not being enabled, not accounting for operating cycle disruptions, and fission energy from plutonium and plutonium production. FIPD use the average LHGRs recorded for a pin to calculate burnup, where BISON uses the average fission rate density of the current and previous timestep (Paaren et al., 2021a).

FISSION gas release

FGR predictions from the BISON simulations were compared to PIE measurements within the IMIS database for 81 of the fuel pins presented, with the other pins using a correlation developed in IMIS (Paaren et al., 2021a). Each of the fuel pins simulated in BISON predicted more FGR than was measured experimentally within the HFEF. Values for the fission gas produced (FGP), fission gas collected (FGC), and FGR fraction predicted from BISON results were compared to the 81 PIE measurements. Other pins used correlations within the IMIS database from these 81 measured pins to estimate FGP, FGC, and FGR percent for other EBR-II fuel pins not selected for measurements. Comparison of these parameters (IMIS estimated vs. BISON predictions) are shown in Figures 4–6. FGC is measured by puncturing the cladding and measuring the pressure differential in a controlled volume. Using the ideal gas law and the temperate of the hot cell, the total number of moles from fission gas production was calculated. Of the fission gas collected, the amount of fission gas produced (including gas still contained within the fuel), is determined by analyzing the number of krypton gas moles released into the controlled volume, and assuming 25% of the fission gas is

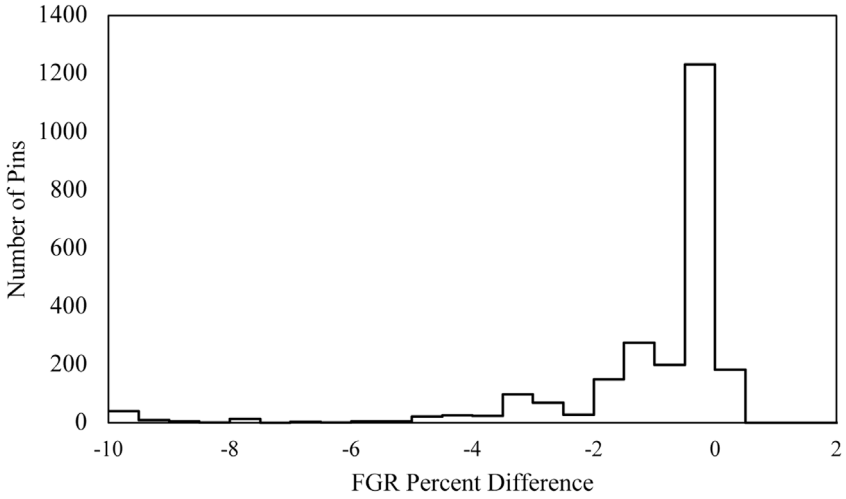

FIGURE 6
Fission gas release comparison (BISON subtracted from FIPD).

retained within the fuel, for both measurements and BISON simulations. Fission gas release percent is simply the ratio of FGC over FGP.

When comparing the values of FGR fraction, FGP, and FGC, between BISON and PIE measurements, FGR values found to be in agreement with BISON underpredicting FGP and FGC. BISON calculates FGP by incorporating porosity and the average fission rate in each element in the U-Pu-Zr FGR material model, but IMIS multiplies the burnup by the number of moles of fissile material in each fuel pin and the fission gas yield fraction to determine the amount of moles from FGP (Hofman et al., 1997). The maximum FGR fraction that BISON simulations can reach is 73.5% and is based on IMIS data. The data itself have considerable scatter and has a non-linear regression R^2 value of 0.67. The BISON simulations represent the IMIS FGR data fairly well, with subtle differences in the FGR fraction. Pins simulated in BISON that differed by more than 2% for FGR had an average burnup less than 1 at %. This is important, as the BISON model does not allow for fission gas to be released from the fuel until terminating porosity is reached, which is speculated to occur between 1-2 at % burnup. Allowing for terminating porosity to occur sooner in BISON would have led to better predictions of FGR for low burnup pins. To increase the accuracy of the BISON model, more FGR experimental measurements need to be performed for both low and high burnup pins to generate a better correlation, such as the data gathered for legacy pins from the FFTF MFF experiments.

Cladding profilometry and fuel axial swelling

Within 29 different experiments simulated, 551 of the pins had cladding profilometry measurements available for BISON comparison, with Figure 7 highlighting BISON's ability to predict cladding strain. For pins with CW316 SS cladding, BISON was able to predict the cladding strain with good agreement, with the highest SEE being 26.5 μm for a CW316 SS pin (J630). This is due to the cladding profilometry being highly dependent on the CW316 SS void swelling and creep models, with FCMI contributing a minimum amount. Both the shape and magnitude of the cladding strain for CW316 SS pins were in agreement. Most of the strain is created by void swelling in the cladding and not entirely dependent upon stresses induced on the cladding by fuel swelling or fission gas pressure. The same cannot be said with D9 cladding pins, with void swelling over and underpredicting cladding strain data. This may be due to lower-numbered experiment (X419—X421) pins not utilizing Germanium-Lithium Argon-Scanning System (GLASS) power history data before operating cycle 139A as it was not available. This allowed for pins irradiated in early operation cycles to utilize effective full power days within the BISON simulations to achieve FIPD fluence values. Although this simulates the FIPD fluence, the temperature history within the fuel and the cladding are averaged over the operating cycle duration, creating lower than expected operating temperatures and discounting important phenomena at higher temperatures, such as creep.

Within Figures 7D, F, the size and profile of the main bulge at fuel centerline (~17 cm) are dependent on the cladding material, cladding temperature, irradiation-induced creep, and the amount of force the fuel is exerting on the cladding at each element. The amount of irradiation creep is indirectly controlled by the axial flux profile used in the BISON simulations and the magnitude of the fast neutron flux. The neutron flux also affects the amount of void swelling in cladding materials in conjunction with temperature. In addition to this, higher burnup pins impart more stress on the cladding though FCMI, allowing for more irradiation and potentially thermal creep. These three effects, when modeled simultaneously, compound and overpredict cladding strain. For the pins in Figures 7D, F, pin T069 and T709 contained plutonium and exceeded burnups of 12 at %. This high burnup and plutonium content simulated increased fuel swelling and anisotropic proportionality constant, leading to the overprediction of cladding strain. The strain seen over the entire cladding wall is due to plenum pressure created from FGR and irradiation-induced creep. For most pins, this is neglected, as the digitized PIE cladding profilometry does not extend for the whole fuel element length, such as T325.

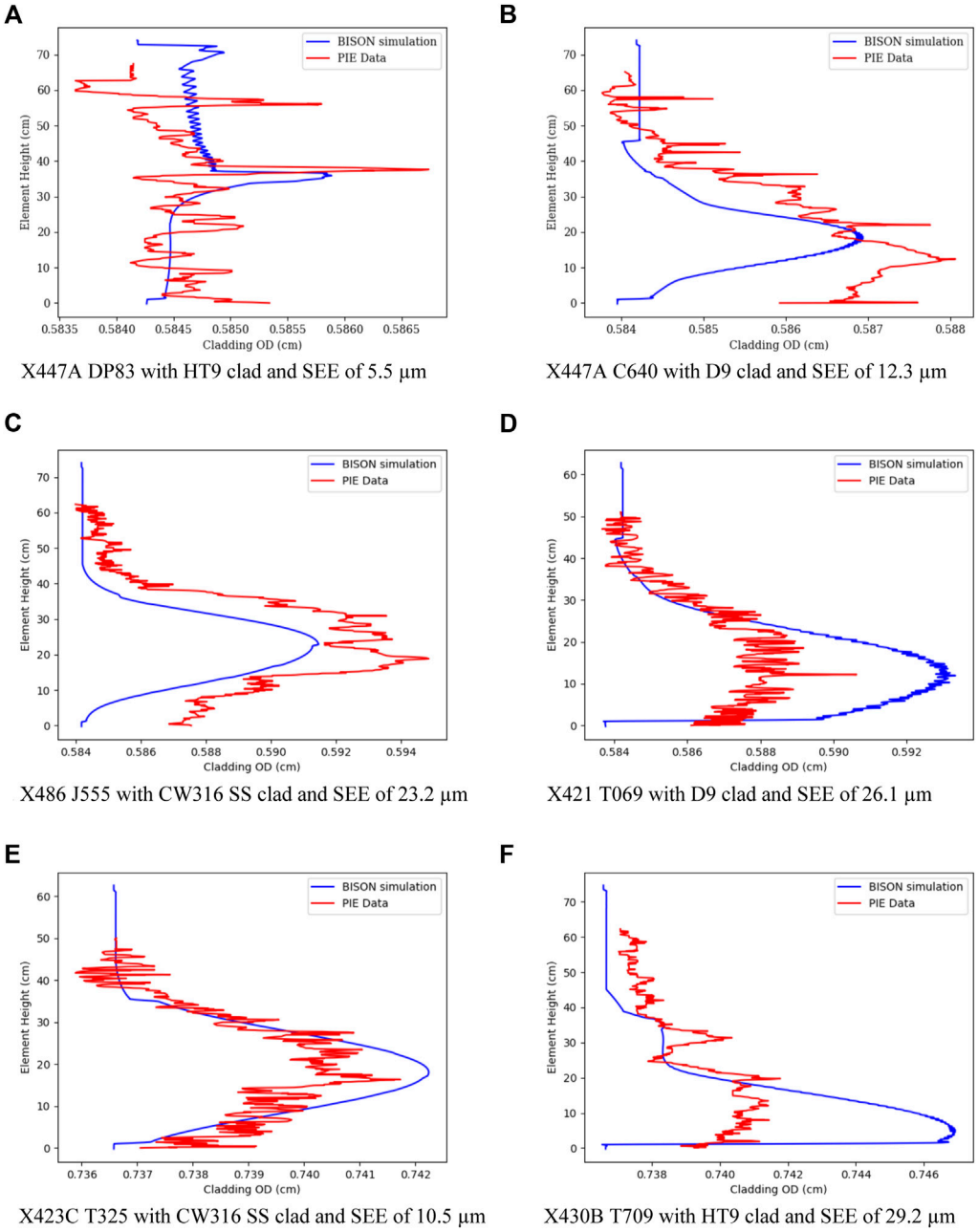

FIGURE 7
Profilometry comparisons of EBR-II fuel pins with various fuel compositions and claddings.

Two examples of cladding profilometry for each cladding type are provided within Figure 7 to show the impact irradiation conditions and different fuel compositions impact fuel performance and profilometry predictions. For the case of HT9 cladding in Figures 7A, F, and upper peak within both PIE measurements and BISON predictions are seen near the top of the fuel (~35–39 cm), which is due to thermal creep. In the case of Figure 7A, pin DP83 underwent a moderate LHGR (~35 $kW{\cdot}m^{-1}$) with a reduced flowrate to increase cladding temperatures. These increased cladding temperatures accelerated FCCI, thermal creep, and increased cladding strain. Pin T709 in Figure 7F had a similar LHGR to DP83 but had plutonium within the fuel in addition to a higher coolant flowrate, larger fuel diameter, and higher burnup. These lower cladding temperatures simulated in Figure 7F allowed for less FCCI and thermal creep, resulting in lower cladding strain near the top of the fuel. In the case of the two SS316 profilometry examples shown in Figures 7C, E, differences between the BISON profilometry predictions are contributed to different irradiation conditions, fuel composition, and fuel diameter.

One fuel performance phenomenon not considered within this modeling scope, due to simulation time, was the addition of a hot-pressing model developed for U-Pu-Zr fuel. This model allows for pore collapse reducing the overall amount of volumetric swelling in the fuel. This would significantly aid pins simulated with SEE values

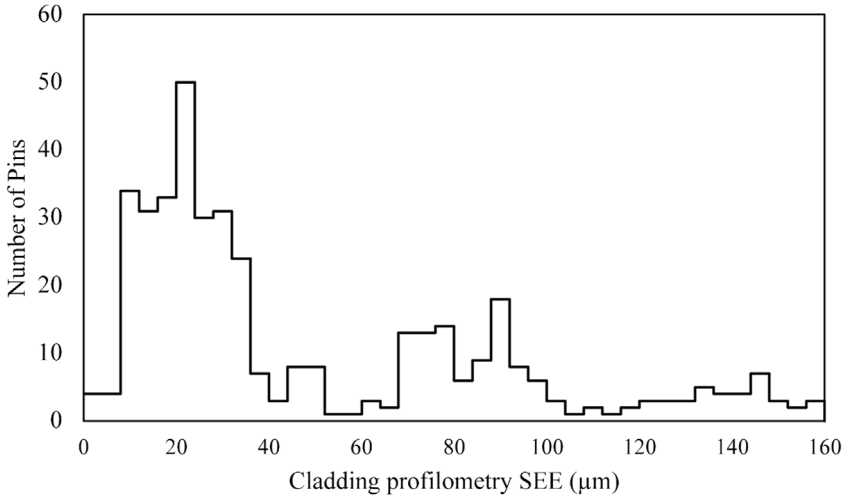

FIGURE 8
Cladding profilometry Standard Error of the Estimate values.

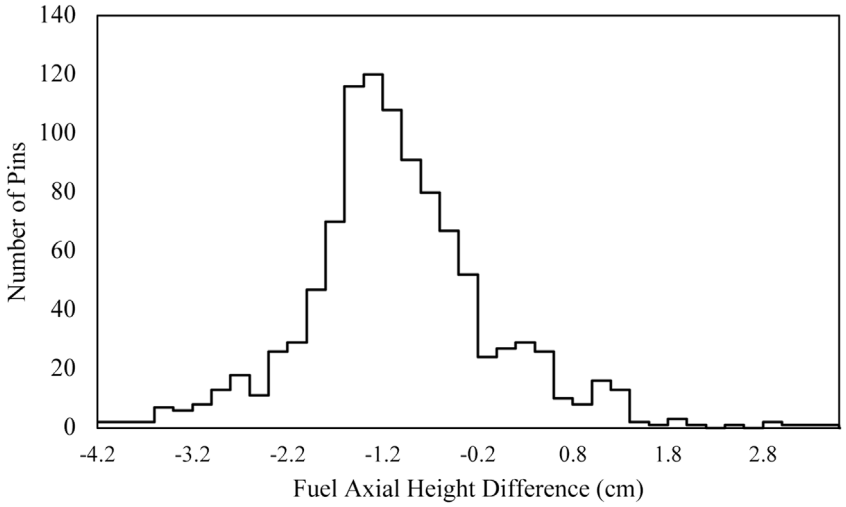

FIGURE 9
Difference in axial fuel swelling length between BISON and Fuels Irradiation and Physics Database (FIPD subtracted from BISON).

greater than 30 μm in Figure 8 (Paaren et al., 2022). Within Figure 8, there are a significant number of pins with SEE values greater than 60 μm, with all being either 85% smeared density, plutonium bearing fuel, or both in the case of DP45 from X441. The high SEE values suggest that the anisotropic swelling proportionality constant is not plutonium dependent, as all plutonium bearing pins overpredicted cladding strain. Removing the anisotropic swelling proportionality constant would decrease SEE values for plutonium bearing pins and increase the axial fuel swelling height, reducing the difference between BISON and PIE measurements in Figure 9.

The friction coefficient used in the simulations also affects the fuel axial swelling, with a friction coefficient greater than 0.2 resisting the axial growth of the fuel (Medvedev, 2012; Hales et al., 2014). The difference in axial fuel height between BISON and PIE measurements is displayed in Figure 9, underpredicting the axial growth of most of the pins by 1.2 cm. In all cases, BISON underpredicts axial fuel lengths of irradiated pins. Implementation of a hot-pressing model for U-Pu-Zr fuel and removal of the anisotropic proportionality constant, in conjunction with zirconium redistribution, would allow for the modulus of elasticity and Poisson's ratio to decrease, allowing for more swelling and creep in the radial direction while limiting overprediction of cladding strain. Efforts are currently being implemented to see how these material models used in conjunction will affect the results produced from a smaller set of BISON EBR-II fuel pin simulations.

Within FIPD, there are unique axial fuel swelling lengths that BISON simulation results may be compared to. Of the unique axial fuel swelling lengths available, some pins contain multiple measurements after each sub-experiment. An example of this is pin T707 containing axial fuel swelling lengths for X430, X430A, and

X430B, each with BISON simulation results to compare to. The axial fuel swelling measurements were subtracted from the corresponding BISON simulations to generate the histogram presented in Figure 9. Note that the histogram contains EBR-II fuel pins with different dimensions, cladding materials, fuel compositions, and irradiation histories although the majority of fuel meat in EBR-II pins had a fabrication height of ~13.5 in. Figure 9 shows in the majority of fuel pins simulated, axial fuel swelling height for the majority of pins was underpredicted, largely due to the direction of swelling controlled by the plutonium-dependent anisotropic proportionality constant. Although only 356 pins within this evaluation contained plutonium, this shows that the fuel swelling material model used in conjunction with the anisotropic proportionality constant does not adequately predict axial fuel swelling. Although the average axial fuel swelling height in BISON simulations is underpredicted by 1.2 cm, this a significant improvement compared to 7 cm overprediction of previous simulations (Medvedev, 2012; Hales et al., 2014).

Discussion

This automated BISON analysis shows it is possible for EBR-II pin information to be supplied in a BISON input file, and simulation results compared to PIE measurements from IMIS and FIPD. This capability serves as the initial benchmark in validating metallic fuel models on a large scale, as well as benchmarking material models in development. The databases used contain the pin dimensions, power history, flux history, axial profiles for power and neutron flux, calculated temperature profiles, coolant channel boundary conditions, burnup calculations, FGR measurements, fuel axial swelling, cladding profilometry, fission product concentrations, and other pin-associated data. The biggest challenge with this work was having discrepancies between fuel pins that utilize the same material and geometric dimensions but contain different resultant PIE measurements. The discrepancies between the BISON simulations and PIE measurements were discussed, along with possible sources of uncertainty within BISON material models, and reactor conditions within IMIS and FIPD.

Since the initial demonstration of linking BISON to IMIS and FIPD for generating EBR-II fuel performance simulations, several new material models have been implemented to enhance BISON's prediction capabilities by describing fuel performance phenomenon using empirical models, such as void swelling of cladding materials, FCCI coupled with damage mechanics for HT9 and D9 cladding, and hot-pressing of the U-Pu-Zr fuel matrix. Each of these, when appended to the BISON general input file, has increased predictions against PIE measurements including cladding strain and axial fuel swelling (Paaren et al., 2021b; Paaren et al., 2021c). However, both the U-Pu-Zr hot-pressing model and the UPuZrGaseousEigenstrain model use an anisotropic proportionality constant to describe the anisotropic swelling nature that is exhibited in Pu-bearing metallic fuels. However, these phenomena can be replicated without the use of this proportionality constant, by including zirconium redistribution into the modeling efforts. This is due to the Young's modulus decreasing with increased plutonium and zirconium content within the fuel matrix, allowing for more creep and deformation in the axial direction when gravity is included in the simulations. The zirconium depletion layer would create a stiff beta-phase matrix relative to the soft gamma and alpha-phase uranium surrounding it. This is represented by correlations in Eqs 15–24 (Hofman et al., 2019).

$$\text{Young's modulus (Pa) } E = E_U{}^*E_T{}^*E_p{}^*E_w \tag{15}$$

$$\text{Pure Uranium at 588 K } E_U = 1.6{}^*10^{11} \tag{16}$$

$$\text{Porosity correction } E_p = 1 - 1.2p \tag{17}$$

$$\text{Weight percent correction } E_w = \frac{1 + 0.17W_{Zr}}{1 + 1.34W_{Zr}} - W_{Pu} \tag{18}$$

$$\text{Temperature correction } E_T = \left(1 - 1.03\left(\frac{T - 588}{T_{mu}}\right)\right) - 0.3f\left(1 - 1.06\left(\frac{T^a_{end} - 588}{T_{mu}}\right)\right). \tag{19}$$

E_U is the Young's modulus for pure uranium at 588 K, E_p is the porosity correction factor, with p being porosity, W_{Zr} and W_{Pu} being zirconium and plutonium weight fractions, p being porosity, and T^a_{end} being the end transition temperature of alpha-phase uranium. The Poisson's ration is adjusted in a similar manner for the fuel matrix, with T_{mu} being the meting temperature of uranium.

$$\text{Poisson's Ratio } V = V_U{}^*V_T{}^*V_p{}^*V_w \tag{20}$$

$$\text{Pure Uranium at 588 K } V_U = 0.24 \tag{21}$$

$$\text{Porosity correction } V_p = 1 - 0.8p \tag{22}$$

$$\text{Weight percent correction } V_w = \frac{1 + 3.4W_{Zr}}{1 + 1.9W_{Zr}} \tag{23}$$

$$\text{Temperature correction } V_T = 1 + 1.2\left(\frac{T - 588}{T_{mu}}\right) \tag{24}$$

In addition to the anisotropic proportionality constant being plutonium dpendent and controlling the direction of the swelling, the total swelling of the fuel, which is modeled being burnup dependent, plays a significant role in FCMI, stresses, and cladding strain. Using a burnup dependent swelling model for 75% smeared density pins leads to overprediction of cladding strain at higher burnups above 8.6 at. %, and underprediction at lower burnups below 8.6 at. %. When simulating higher smeared density pins, such as 85% smeared density pins from X441, simulated cladding strain was overpredicited at lower and higher burups (4 at % and 8.6 at. %). This shows the need to implement a porosity collapse model based off FCMI stress and creep rate used in previous work (Paaren et al., 2021b; Paaren et al., 2021c).

Other modeling characteristics that may cause discrepancies between the BISON simulations and the PIE measurements is the uncertainty of the reactor operating conditions, including reactor power, fluence, and flowrate conditions. As shown in previous work, a fluctuation in base power can significantly affect fuel performance predictions (Galloway et al., 2015; Paaren et al., 2021c). In addition to the uncertainty within reactor power, EBR-II reactor power history is not available for operating cycles before 139A and after 167A. This leads to relying on the FIPD average LHGR values for each of those operating cycles, leaving out important temperature-dependent fuel performance phenomenon that would otherwise be captured if power oscillations were included. This simplification only impacts low and high numbered EBR-II experiments, such as X421 and X496.

While this paper is intended to demonstrate the direct connection of high-fidelity fuel performance modeling using BISON with a large experimentally obtained database to evaluate fuel performance models

for metallic fuel, this study revealed sophisticated interplay of the different phenomena previously described in the literature, but never coupled together. Specifically, that the implementation of U-Pu-Zr hot-pressing and zirconium redistribution need to be coupled together in general metallic fuel modeling and evaluated against the IMIS and FIPD databases to assess the improvement.

The BISON results presented in evaluating metallic fuel models used input conditions from FIPD to produce fuel performance predictions and compared them to PIE measurements. Each PIE parameter acted as a validation check for the BISON simulation results, where the BISON results are highly dependent on modeling parameters chosen in the input files and the reactor conditions supplied by the database. This large comparison shows that uncertainty analysis is needed in addition to incorporating new material models for a better benchmark with the EBR-II data. This would remove the need for proportionality constants such as anisotropic proportionality constant from the code. Depending on the proportionality constants used within BISON, different BISON input files can be statistically fitted to PIE measurements. This shows the need to have defined input parameters for various metallic fuel models to yield the best quantitative results. This is difficult to evaluate because the BISON code is constantly changing due to new material models being committed.

Conclusion

The purpose of this work was to evaluate metallic fuel performance predictions from the BISON code against experimental data contained within the IMIS and FIPD databases, measured from pins out of in-reactor experiments. Here, all 1,977 unique pins within FIPD were modeled within BISON to produce simulation results validated with PIE comparisons. The BISON simulations coupled with IMIS and FIPD have proven successful in predicting average burnup for metallic fuel pins irradiated in EBR-II, but underpredict peak burnup values compared to the data in IMIS and FIPD. Cladding profilometry, fission gas behavior (FGR, FGP, and FGC), and axial fuel swelling were examined as well then compared to PIE measurements within the databases. Cladding profilometry was evaluated using SEE to determine the fitment of BISON-predicted profilometry to the PIE profilometry measurements. Agreement was seen between CW316 SS clad pins, with D9 and HT9 clad pins both overpredicting and underpredicting FCMI and cladding strain at higher burnups. The FGR for the BISON simulations were in agreement with PIE measurements, but more experimental measurements for both very low and high-burnup metallic fuel pins need to be performed to further optimize the BISON model for FGR in U-Pu-Zr fuel. Axial fuel swelling predicted by BISON underrepresented the PIE measurements by ~1.2 cm for most pins. With BISON overpredicting cladding strain and underpredicting axial fuel swelling, a combination of models influencing fuel swelling should be explored. Additionally, the uncertainty of in-reactor operating conditions and empirical material models should be considered when evaluating metallic fuel performance. This modeling work shows that BISON simulations may be created and evaluated using IMIS and FIPD data to compare corresponding PIE measurements for benchmarking and validating advances in metallic fuels and changes to the BISON code. As models become more advanced and the BISON code evolves by using this process for inspection, this tool will be adapted to validate new metallic fuel models.

Data availability statement

The original contributions presented in the study are included in the article/supplementary material, further inquiries can be directed to the corresponding author.

Author contributions

KP: Conceptualization, Methodology, Software, Validation, Formal analysis, Investigation, Resources, Data Curation, Writing—Original Draft, Preparation, Writing—Review and Editing, Visualization MG: Writing—Review and Editing, Supervision, Project administration, Funding acquisition Pavel Medvedev: Writing—Review and Editing, Supervision, Project administration, Funding acquisition DP: Resources, Writing—Review and Editing, Supervision, Project administration, Funding acquisition.

Funding

This research made use of the resources of the High Performance Computing Center at Idaho National Laboratory, which is supported by the Office of Nuclear Energy of the U.S. Department of Energy and the Nuclear Science User Facilities under Contract No. DE-AC07-05ID14517.

Acknowledgments

The authors acknowledge Adam X. Zabriskie, Stephen R. Novascone, Nancy J. Lybeck, Aaron Oaks, Kun Mo, and Abdellatif Yacout for providing review input, knowledge, and experimental data.

Conflict of interest

The authors declare that the research was conducted in the absence of any commercial or financial relationships that could be construed as a potential conflict of interest.

The handling Editor declared a shared affiliation with the authors at the time of review.

Publisher's note

References

Altenbach, H., and Gorash, Y. (2013). *Advanced materials modelling for structures*. 1st. Verlag Berlin Heidelberg: Springer.

American Society of Mechanical Engineers (2016). *ASME boiler and pressure vessel code*. New York, NY: Boiler and Pressure Vessel Committee

Banerjee, A., Raju, S., Divakar, R., and Mohandas, E. (2007). High temperature heat capacity of alloy D9 using drop calorimetry based enthalpy increment measurements. *International Journal of Thermophysics*, 28, 1, 97–108. doi:10.1007/s10765-006-0136-0

Billone, M. C., Liu, Y. Y., Gruber, E. E., Hughes, T. H., and Kramer, J. M. (1968). "Status of fuel element modeling codes for metallic fuels," in Proceedings American Nuclear Society Internaionl Conference on Reliable Fuels for Liquid Metal Reactors. Beijing China

Briggs, L. L., Il Chang, Y., and Hill, D. J. (1995). *Safety analysis and technical basis for establing an interim burnup limit for mark-V and mark-VA fueled subassemblies in EBR-II*. Argonne National Lab. ANL, Argonne, IL

Carmack, W. J. (2012). *Temperature and burnup correlated fuel-cladding chemical interaction in U-10Zr metallic fuel*. University of Idaho. Moscow, ID, USA

Cohen, J. (1988). *Statistical power analysis for the behavioral sciences*. Department of Psychology University NY China 2nd.

Crawford, D. C., Steven, L., and Powers, J. J. (2018). A proposed startup fuel for the versatile test reactor. *Trans. Am. Nucl. Soc.* 118.

Everitt, B. S., and Skrondal, A. (2010). *The cambridge dictionary of statistics*. 4th. New York: Cambridge University Press.

Fink, J. K., and Leibowitz, L. (1995). *Thermodynamic and transport properties of sodium liquid and vapor*. Argonne, Illinois.

Galloway, J. D. (2015). Fully-coupled metallic fuel performance simulations using BISON. *LA-UR* 15-26773.

Galloway, J. D., and Matthews, C. (2016). Enhancements to BISON U-Zr metallic fuel X447 example problem. https://www.osti.gov/biblio/1329651

Galloway, J., Unal, C., Carlson, N., Porter, D., and Hayes, S. (2015). Modeling constituent redistribution in U-Pu-Zr metallic fuel using the advanced fuel performance code BISON. *Nucl. Eng. Des.* 286, 1–17. doi:10.1016/j.nucengdes.2015.01.014

Garner, F. A., and Porter, D. L. (1988). Irradiation creep and swelling of AISI 316 to exposures of 130 dpa at 385-400 C. *J. Nucl. Mat.* 155, 1006–1013. doi:10.1016/0022-3115(88)90458-8

Garner, F. A. (2017). Swelling, creep and embrittlement of D9 stainless steel cladding and duct irradiated in three FFTF driver fuel assemblies to high neutron exposures. *Twelfth Int. Ural. Semin. Radiat. Damage Phys. Mater. alloy. Abstr.* 109.

GeelHood, K. J., and Porter, I. E. (2018). Modeling and assessment of EBR-II fuel with the US NRC's fast fuel performance code. *Proc. Top Fuel* 12.

Hales, J. D., and Zhao, M. (2015). BISON users manual - BISON release 1. *Ida. Falls* 2.

Hales, J. D., Novascone, S. R., Spencer, B. W., Williamson, R. L., Pastore, G., and Perez, D. M. (2014). Verification of the BISON fuel performance code. *Ann. Nucl. Energy* 71, 81–90. doi:10.1016/j.anucene.2014.03.027

Hofman, G. L., Billone, M. C., Koenig, J. F., and Kramer, J. M. (2019). *Metallic fuels handbook*. NY China

Hofman, G. L., Walters, L. C., and Bauer, T. H. (1997). Metallic fast reactor fuels. *Prog. Nucl. Energy* 31 (1), 83–110. doi:10.1016/0149-1970(96)00005-4

Karahan, A., and Buongiorno, J. (2010). A new code for predicting the thermo-mechanical and irradiation behavior of metallic fuels in sodium fast reactors. *J. Nucl. Mat.* 396, 283–293. doi:10.1016/j.jnucmat.2009.11.022

Karahan, A. (2010). *Modeling of thermo-mechanical and irradiation behavior of mixed oxide fuel for sodium fast reactors*. Massachusetts Institute of Technology. Cambridge, MA

Leibowitz, L., and Blomquist, R. A. (1988). Thermal conductivity and thermal expansion of stainless steels D9 and HT9. *Int. J. Thermophys.* 9, 873–883. doi:10.1007/bf00503252

Los Alamos National Laboratory (2014). AFCI materials handbook, materials data for particle accelerator applications, chapter 18 - Design properties of HT9 and Russian ferritic/martensitic steels. *Rev* 6.

Matthews, C., Galloway, J., Unal, C., Novascone, S., and Williamson, R. (2017). BISON for metallic fuels modelling, https://inis.iaea.org/collection/NCLCollectionStore/_Public/48/088/48088059.pdf, IAEA-CN245-366

Mills, Kenneth C. (2002). *Recommended values of thermophysical properties for selected commercial alloys*. Woodhead Publishing. Sawston, Cambridge

Niffenegger, M., and Reichlin, K. (2012). The proper use of thermal expansion coefficients in finite element calculations. *Nucl. Eng. Des.* 243, 356–359. doi:10.1016/j.nucengdes.2011.12.006

Oaks, A., Mo, K., Mohamed, W., and Yacout, A. (2019). "Development of FIPD: The EBR-II fuels irradiation and physics database," in Proceedings of the Top Fuel 2019: lIght Water Reactor Fuel Performance Conference, Beijing China.

Ogata, T., and Takeshi, Y. (1999). Development and validation of ALFUS: An irradiation behavior analysis code for metallic fast reactor fuels. *Nucl. Technol.* 128, 113–124. doi:10.13182/nt99-1

Olander, D. R. (1976). *Fundamental aspects of nuclear reactor fuel elements*. Technical Information Center, Energy Research and Development Administration. Souel Korea

Paaren, K. M., and Chen, L. (2021). BISON fuel performance modeling optimization for experiment X447 and X447A using axial swelling and cladding strain measurements. *Nucl. Eng. Des.* 10.

Paaren, K. M., Gale, M. D., Medvedev, P. G., and Porter, D. L., "Fuel performance analysis of fast flux test facility MFF-3 and -5 fuel pins using BISON with post irradiation examination data," *J. Nucl. Mat.*, vol. TBD, no. TBD, p. 16, 2022.

Paaren, K. M., Gale, M., Kerr, M. J., Medvedev, P. G., and Porter, D. L. (2021). Initial demonstration of Automated fuel performance modeling with 1,977 EBR-II metallic fuel pins using BISON code with FIPD and IMIS databases. *Nucl. Eng. Des.* 37, 1,

Paaren, K. M., Lybeck, N., Mo, K., Medvedev, P. G., and Porter, D. L. (2021). Cladding profilometry analysis of experimental breeder reactor-II metallic fuel pins with HT9, D9, and SS316 cladding. *Energies* 14, 515. doi:10.3390/en14020515

Medvedev, P. G., "Fuel performance modeling results for representative FCRD irradiation experiments: Projected deformation in the annular AFC-3A U-10Zr fuel pins and comparison to alternative designs," *Ida. Natl. Lab. Rep.*,) 13 no. September, p. INL/EXT-12-27183, 2012, doi:10.2172/1091354

Porter, D., and Mariani, R. D. (2019). *Archiving EBR-II metallic fuel test data using NDMAS to accelerate fast reactor fuel qualification*. United States: Idaho National Lab.

Savage, H. (1968). The heat content and specific heat of some metallic fast-reactor fuels containing plutonium. *J. Nucl. Mat.* 25 (3), 249–259. doi:10.1016/0022-3115(68)90168-2

V Gribok, A., Porter, D. L., Paaren, K. M., Gale, M. D., Middlemas, S. C., and Lybeck, N. J. (2021). Automatic information extraction from neutron radiography imaging to estimate axial fuel expansion in EBR-II. *J. Nucl. Mat.* 557–153250. doi:10.1016/j.jnucmat.2021.153250

Williamson, R. L., Gamble, K., Perez, D., Novascone, S., Pastore, G., Gardner, R., et al. (2016). Validating the BISON fuel performance code to integral LWR experiments. *Nucl. Eng. Des.* 301, 232–244. doi:10.1016/j.nucengdes.2016.02.020

Williamson, R. L., Hales, J. D., Novascone, S. R., Pastore, G., Gamble, K. A., Spencer, B. W., et al. (2021). BISON: A flexible code for advanced simulation of the performance of multiple nuclear fuel forms. *Nucl. Technol.* 207, 954–980. doi:10.1080/00295450.2020.1836940

Yacout, A. M., Oaks, A., Mohamed, W., and Mo, K. (2017). Fipd: EBR-II fuels irradiation and physics database. https://www.osti.gov/biblio/1480520

Yacout, B. A. M., and Billone, M. C. (2017). Pre-licensing evaluation of legacy SFR metallic fuel data. *ANL-ART* 76.

Yamanouchi, N., Tamura, M., Hayakawa, H., and Kondo, T. (1992). Accumulation of engineering data for practical use of reduced activation ferritic steel: 8%Cr-2%W-0.2%V-0.04%Ta-Fe. *J. Nucl. Mat.* 191–194, 822–826. doi:10.1016/0022-3115(92)90587-b